ACS OMEGA

http://pubs.acs.org/journal/acsodf

Article

Rheological Response of Polylactic Acid Dispersions in Water with Xanthan Gum

Sara Buoso, Giada Belletti, Daniele Ragno, Valter Castelvetro, and Monica Bertoldo*

Cite This: *ACS Omega* 2022, 7, 12536−12548

Read Online

ACCESS | Metrics & More | Article Recommendations | Supporting Information

ABSTRACT: In this work, the rheological behavior of stable poly(lactic acid) (PLA) dispersions in water, intended for coating applications, was investigated. The newly prepared dispersion consists of PLA particles with an average diameter of 222 ± 2 nm based on dynamic light scattering (DLS) and scanning electron microscopy (SEM) analyses, at concentrations varying in the 5−22 wt % range. Xanthan gum (XG), a bacterial polysaccharide, was used as a thickening agent to modulate the viscosity of the formulations. The rheological properties of the PLA dispersions with different XG and PLA contents were studied in steady shear, amplitude sweep, and frequency sweep experiments. Under steady shear conditions, the viscosity of all the formulations showed a shear-thinning behavior similar to XG solutions in the whole investigated 1−1000 s^{-1} range, with values dependent on both PLA particles and XG concentrations. Amplitude and frequency sweep data revealed a weak-gel behavior except in the case of the most diluted sample, with moduli dependent on both PLA and XG contents. A unified scaling parameter was identified in the volume fraction (ϕ) of the PLA particles, calculated by considering the dependence of the continuous phase density on the XG concentration. Accordingly, a master curve at different volume fractions was built using the time−concentration−superposition approach. The master curve describes the rheological response of the system over a wider frequency window than the experimentally accessible one and reveals the presence of a superimposed β relaxation process in the high-frequency region.

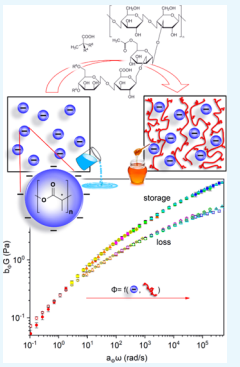

1. INTRODUCTION

Poly(lactic acid) (PLA) is an aliphatic polyester derived from renewable sources, such as corn starch and sugarcane. It is considered one of the most promising candidates to replace many petroleum-based polymers.[1] In addition to the good mechanical properties, such as high tensile strength and stiffness, and easy processability, it is also biodegradable, biocompatible, and nontoxic. It is mainly used in biomedical applications (e.g., for sutures, clips, and drug delivery systems) and in food packaging (bottles, sheets, films, and extruded coatings).[2] Usually, PLA is converted into items through melt processing, which can be considered environmentally benign as it does not involve the use of organic solvents. However, by this route, it is not possible to prepare very thin coating layers (<100 μm). On the contrary, minimal coating thickness (<20 μm) is often desired to reduce material consumption and thus the environmental impact as well as the cost of the items. Thin PLA coatings have been prepared by solvent casting, hot pressing, or electrospinning methodologies.[2,3] Despite the huge interest in water-based coatings, only a few studies account for the preparation of PLA dispersions in water.[4−6] Furthermore, in most of them, halogenated solvents are employed to solubilize the polymer during the preparation of the aqueous dispersion, preventing further use in many applications, in particular the food contact ones.[6] An effective and environmentally friendly method to prepare PLA aqueous dispersions suitable for many applications, including thin coatings for food packaging, has been recently developed by our group.[5] The preparation strategy provides very stable dispersions that can be stored for several months and later used to prepare films and coatings.[7] The thickness of polymeric coatings prepared from water dispersions can be controlled through the concentration (dry matter content) and the viscosity of the same. The correlation with viscosity is quite complex and depends on the rheological response under shear and on the actual shear rate during the application, which in turn depends on the specific application technology and on the processing parameters.[8] In addition to film thickness, the response to deformation and flow under shear affects other application-relevant properties.[9] In particular, dispersion coatings need to have high viscosities in the low shear region to avoid settling and instability during storage and transport. On the other hand, they need to have low viscosities in the high shear rate region, which corresponds to the application.[10] Furthermore, the time-dependent viscosity buildup after exposure to high shear should be fast enough to prevent sagging but still slow enough to allow good flow leveling. Usually, suitable rheology control is achieved with specific additives.[11] Thickeners are

Received: September 28, 2021
Accepted: January 24, 2022
Published: April 6, 2022

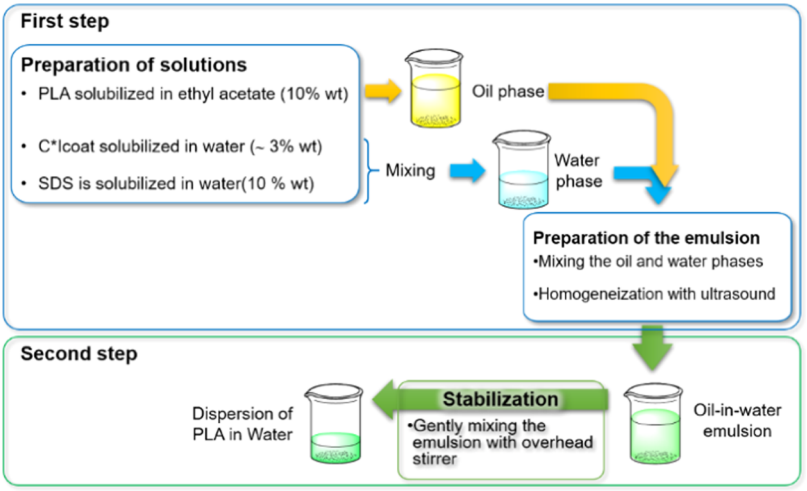

Figure 1. Cartoon of the procedure for the preparation of the PLA dispersion in water.

rheological additives acting as viscosity-enhancing substances that build up structures in a solution through their interaction with water and/or dispersed particles.[10] The industrially relevant thickeners for coating applications are cellulose ethers, polyurethanes, and polyacrylates. The latter two are non-biodegradable polymers mainly produced from fossil oil. Cellulose ethers, obtained by chemical modification of the naturally occurring cellulose, can be either biodegradable or not, depending on the modification degree. A fully biodegradable alternative is xanthan gum (XG), a high molecular weight branched polysaccharide produced by fermentation of Xanthomonas Campestris.[12] XG has the same β-(1 → 4)glucopyranose backbone as cellulose, but with additional negatively charged trisaccharide sidechains linked to every other main-chain glucopyranose ring with α-1,3 linkage. The trisaccharide branches consist of a β-D-glucuronic acid residue between two D-mannose residues. Approximately, one-half of the D-mannose side-chain terminals bearing, with unknown distribution, a pyruvic acid residue is linked via a keto group to the 4 and 6 positions, while the inner D-mannose unit carries an *O*-6-acetyl group.[12] This biopolymer is nontoxic and forms hydrocolloidal solutions with high stability at high shear values and in a wide range of pH, temperature, and ionic strength.[13,14] Such branched polyelectrolyte chains can build up a network even at low concentrations; thus, xanthan solutions show a pseudoplastic behavior with predominant conservative properties.[15−18] However, while at low frequencies the predominance of the elastic (G') over the viscous (G'') modulus is similar to the behavior of a gel, XG is a nongelling agent when it is used alone; thus, its solutions retain the flow properties required for their effective spreading over surfaces.[19] XG is commonly used as a rheology modifier in food,[20,21] cosmetic, agricultural, pharmaceutical,[22] and petroleum industry applications,[14,19] as well as in home- and personal care product formulations.[23] However, to the best of our knowledge, it has not been proposed yet for industrial coating use. On the contrary, in spite of its relatively high price, XG may be considered as an interesting sustainable alternative to the current waterborne coating additives because of its effectiveness as a thickener at very low concentrations.[21,24] Typical shear rate values for coating, painting, brushing, and spraying processes are in a range between 10^2 and 10^5 s^{-1}.[25] The highest limit is not accessible with many of the commonly available instruments for rheological characterization even in research laboratories. To overcome these limits, there are indirect methodologies that account for the behavior of the studied system at such high values. The time−temperature−superposition (TTS)[26] and time−concentration−superposition (TCS)[27] principles are among the most employed indirect methods: they consist of superposing viscoelastic curves registered at different temperatures (TTS) or at different concentrations (TSC), with respect to a reference curve. The obtained result is the so-called master curve. It extends over a range of frequencies (or times) much larger than those directly accessible to the experimental setup.[27−33] Note that while the TTC approach has been fully elucidated from a theoretical point of view, TCS has not been yet. Nevertheless, it is common to name TCS as a principle. The aim of this work was to study the possibility of using XG as a biodegradable thickener for water dispersions of PLA, so as to allow the preparation of coatings made of more than 90% biodegradable components. Once the possibility to incorporate XG in the PLA emulsion had been assessed, the study was focused on finding out a possible correlation between composition and rheological response. It is worth emphasizing that the system described here is the first example ever of a water-based colloidal PLA dispersion. On the contrary, previous rheological studies involving PLA dispersions have been limited to highly viscous polymer melts in which the polyester was the matrix and the filler was the dispersed phase, aiming at a particle-modified PLA-based material.[34,35] Here, both the viscosity and the viscoelastic behavior of aqueous PLA/XG dispersions were studied at different compositions, where the concentration of both the dispersed phase and the aqueous XG matrix were independently varied. The time−concentration principle was then applied to cover a wider range of frequencies.

2. RESULTS

2.1. Preparation and Characterization of the PLA Dispersion. A water dispersion of amorphous PLA in water, stabilized with starch and sodium dodecyl sulfate (SDS) as an emulsifier, was prepared by a two-step procedure, as sketched in Figure 1, and was previously reported by us.[7]

In the first step, an organic phase was prepared by dissolving PLA in ethyl acetate, and an aqueous phase by solubilizing SDS and starch in ultrapure water. The two phases were mixed,

https://doi.org/10.1021/acsomega.1c05382
ACS Omega 2022, 7, 12536−12548

homogenized by sonication, and then the organic solvent was distilled off under moderately reduced pressure. The obtained dispersion, with 15.0 ± 0.1% dry matter content, appears as a white, homogenous, clots-free liquid with water-like viscosity (Table 1; D0_15). Dynamic light scattering (DLS) analysis of the dispersion revealed sub-micrometer-sized particles with an average hydrodynamic diameter of 222 ± 2 nm and polydispersity of 0.230 ± 0.003 (Figure 2a). A comparable size could be observed by scanning electron microscopy (SEM) analysis of the dried particles obtained from the dispersion (Figure 2b).

Table 1. Prepared Dispersions of PLA/XG with Given C_X Concentrations of XG and C_P Concentrations of PLA in Water

acronym[a]	C_X (wt %)	C_P (wt %)[b]
D0_15	0	15.00 ± 0.10
D15_15[c]	0.151	15.25 ± 0.08
D25_15[c]	0.251	15.35 ± 0.10
D35_15[c]	0.356	15.45 ± 0.11
D50_15[c]	0.503	15.60 ± 0.06
D65_15[c]	0.655	15.76 ± 0.09
D75_15[c]	0.760	15.86 ± 0.10
D50_5[d]	0.50	5.02 ± 0.03
D50_10[d]	0.50	10.02 ± 0.08
D50_12.5[d]	0.50	12.5 ± 0.10
D50_13.5[d]	0.50	13.5 ± 0.03
D50_20[d]	0.50	22.29 ± 0.10
D75_5[d]	0.75	4.99 ± 0.09
D75_10[d]	0.75	9.98 ± 0.05
D75_20[d]	0.75	20.25 ± 0.07

[a]Samples are labeled with the acronym D*x*_*p*, where *x* represents the concentration of XG in wt % multiplied by 100, and *p* represents the concentration of PLA particles in wt %. [b]Determined as weighed dry residue (see the Experimental Section). [c]Dispersions prepared by varying the amount of XG added at constant dry residue. [d]Dispersions prepared by varying the dry residue at a fixed amount of XG (0.50 or 0.75 wt %).

The negative *Z* potential of −35.30 ± 0.85 mV (Table S2), as expected from the presence of the anionic SDS surfactant on the particle's surface, resulted in the high stability of the dispersion. Indeed, no evidence of the onset of either coagulation or sedimentation processes was visually detectable over 6 months of storage both at room temperature and at 4 °C (Figure 3).

The DSC analysis of the polymeric material obtained upon drying the dispersion showed a glass transition temperature T_g = 54 °C, close to that of the pristine PLA 4060D (T_g = 58 °C) used to prepare the dispersion. Neither melting nor crystallization was detected, in agreement with the fully amorphous structure declared for the pristine polymer.[36,37] A small peak at ∼195 °C, detected during the first DSC heating step (Figure S1), cannot be attributed to PLA as its maximum reported melting temperature is 178 °C for the semicrystalline homopolymer of the 100% L-lactide stereoisomer.[38] The mentioned endotherm could rather be attributed to the degradation of some minor components or to the evaporation of trapped water, linked to the starch component in the dispersion.[39] Accordingly, TGA analysis revealed a minor weight loss (about 1.5 wt % at 195 °C) process occurring just before the onset, at about 200 °C, of the first of the two main degradation steps (Figure S2).

No detectable difference in the PLA molecular weight and molecular weight dispersity could be detected by GPC analysis when comparing the pristine PLA and the product obtained from the dispersion (Table S3), indicating the absence of significant hydrolysis of the polyester during the ultrasound processing in the water phase.

2.2. Addition of XG to the PLA Dispersion. The addition of XG as a thickener to the PLA dispersions (Table 1) did not result in any appreciable change in their apparent

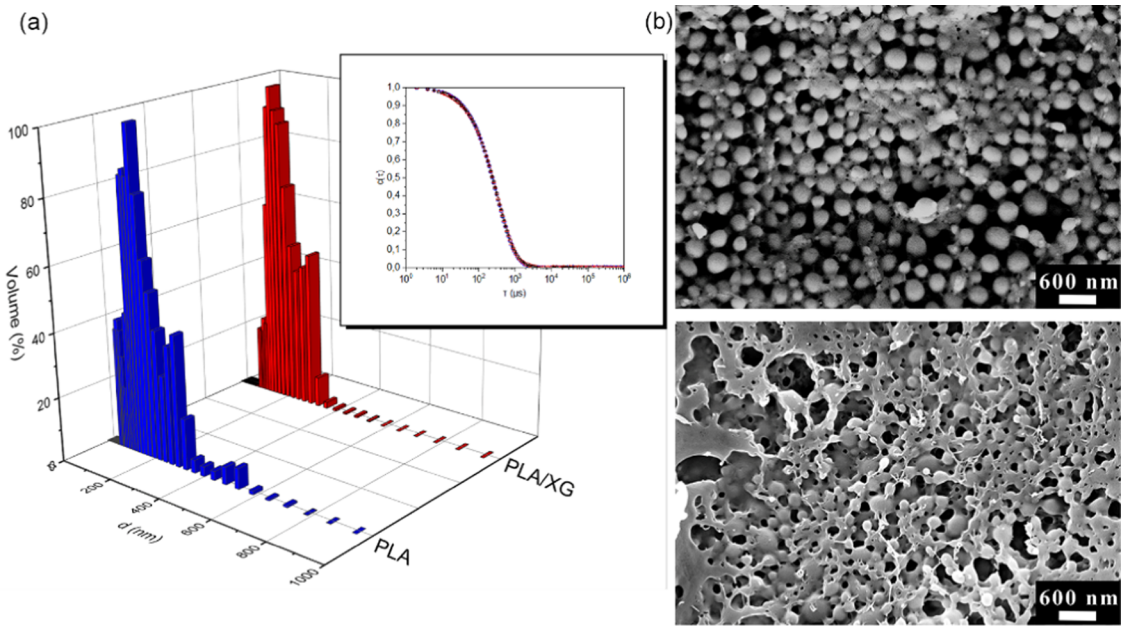

Figure 2. (a) DLS size distribution plots of PLA dispersions without xanthan gum (D0_15, blue histogram) and with 0.35 wt % xanthan gum (D35_15, red histogram); inset: DLS correlation plots of the same dispersions. (b) SEM micrographs of D0_15 (top) and D35_15 (bottom) dispersions at 40k magnification. Error bars are calculated as standard deviation (eq 8).

https://doi.org/10.1021/acsomega.1c05382
ACS Omega 2022, 7, 12536−12548

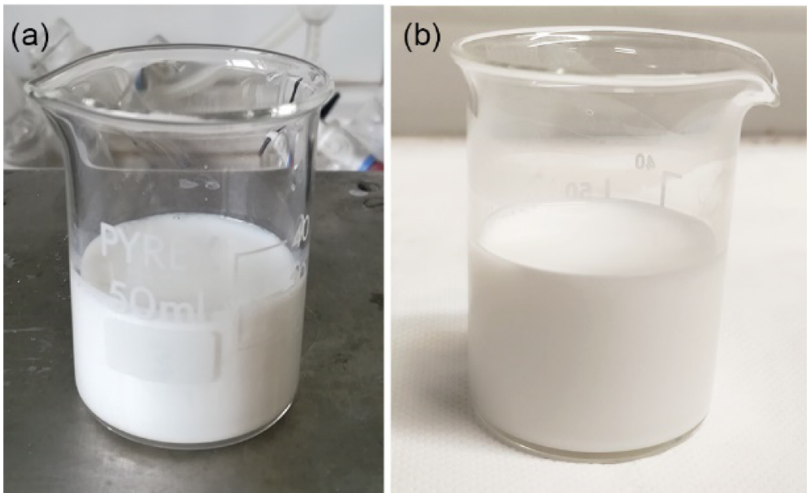

Figure 3. Pictures of the PLA dispersion D0_15 just prepared (a) and after 6 months (b).

properties, except for the higher viscosity. No creaming, sedimentation, or coagulation formation was detected over a few months of observation, indicating that XG does not negatively affect the dispersion stability. Accordingly, the DLS correlation plots obtained from the dispersions with added XG are overlapping with those from the corresponding pristine PLA dispersions (inset in Figure 2a): the DLS correlation curve shows a single inflection point, suggesting the absence of large clusters or of secondary phase domain formation. Particle size distribution by volume is almost bimodal for both dispersion types (with and without XG, Figure 2a). The average particle size and polydispersity were found to not appreciably depend on either XG or particles' concentration (Table S1).

The addition of XG confers to the initial PLA dispersion a typical honey-like viscosity, a feature that will be discussed in-depth in the next section. SEM analysis of the dried PLA/XG dispersion shows a densely interconnected pattern (Figure 2b), likely associated with the buildup of an interconnected network between XG and nanoparticles. Individual particles are still detectable but they are held together by XG resulting in a biphasic morphology. The presence of such a network becomes more evident at increasing XG/PLA mass ratio (Figure S3a). Indeed, when the concentration of PLA decreases, its particles are hardly detectable within the XG network (Figure S3b).

Even in the presence of XG, the molecular weight ($\bar{M}_n$) and dispersity of PLA were comparable to those of the pristine polymer (Table S3), an indication of the absence of any degradation phenomena throughout all the preparation steps, including the addition of the XG thickener.

2.3. Steady Shear Properties of PLA/XG Dispersions.

Neat PLA dispersions in water show, within the concentration range of our interest, viscosity independent of the shear rate and similar to water (Figure 4), as typically observed for low concentration of hard-sphere colloids.[40] On the contrary, when XG is added to the dispersion it conveys a shear-thinning behavior, and the Newtonian plateau is no longer observed. The flow curve profiles of the thickened dispersion show the same features as those of aqueous XG solutions (see Figure S4a in the supporting information), a behavior previously observed for aqueous dispersions of SiO_2 particles with XG.[41] However, the viscosity of the PLA/XG dispersion is higher

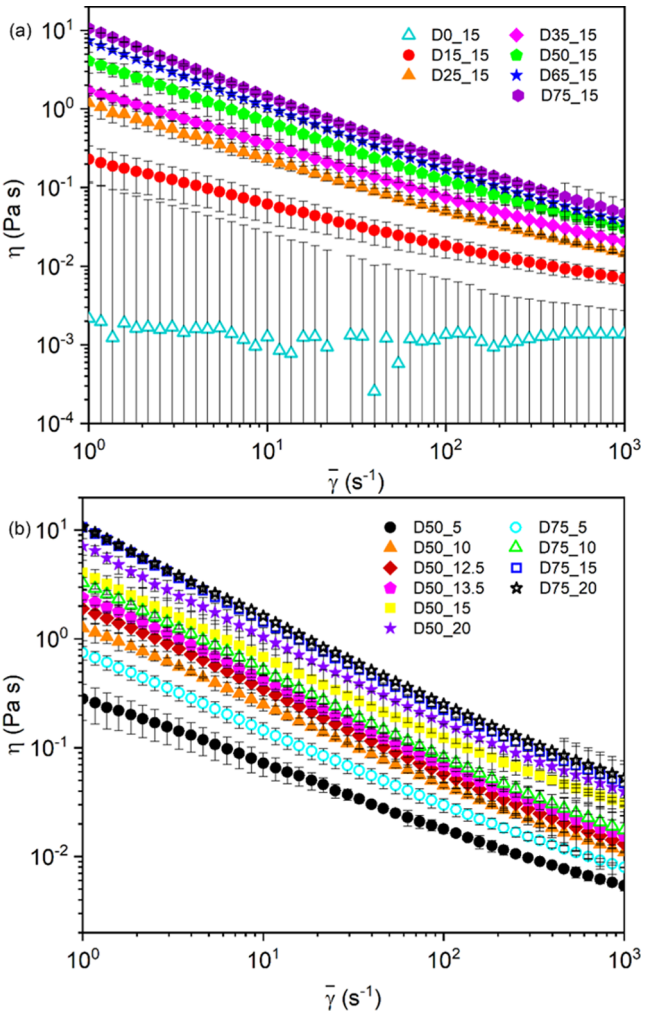

Figure 4. Viscosity as a function of shear rate for dispersions with (a) different concentrations of XG and constant content of particles; (b) different concentrations of particles and constant concentration of XG. See Table 1 for the decoding of the acronyms in the legend. Error bars are calculated as standard deviation (eq 8).

(Figure S4b) than that of the reference XG solution. The increase of viscosity is higher than that expected from a simple additive contribution by the viscosity of the neat PLA

https://doi.org/10.1021/acsomega.1c05382
ACS Omega 2022, 7, 12536−12548

dispersion. This indicates the occurrence of specific interactions between the particles and the polysaccharides. Accordingly, the viscosity of the PLA/XG mixed dispersions increases by increasing either the XG or the PLA particle concentrations, with comparable dependence on the shear rate at all investigated compositions (Figure 4).

2.4. Dynamic Viscoelastic Properties of PLA/XG Dispersions. Amplitude sweep experiments performed on samples with different concentrations of PLA or XG show, as expected, a low strain sweep region in which both storage and loss moduli are constant (Figure 5). In this region, the former

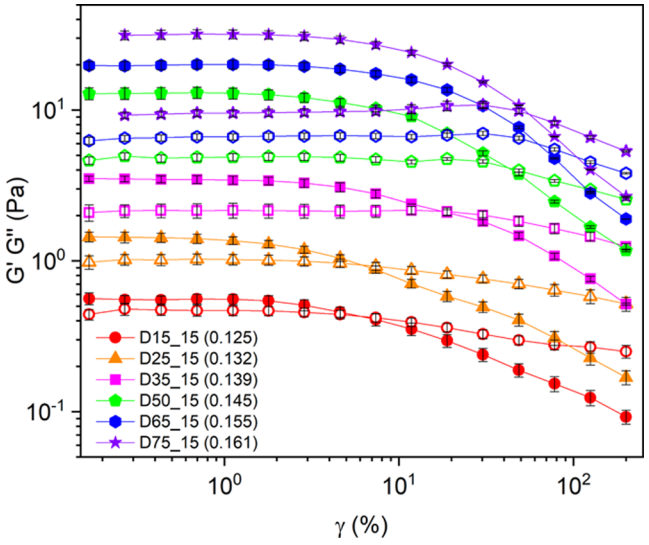

Figure 5. Storage (G'—full symbols) and loss (G''—empty symbols) moduli as a function of strain sweep for dispersions with 15 wt % PLA particles and different XG concentrations (circles: 0.15, triangles: 0.25, squares: 0.35, pentagons: 0.50, hexagons: 0.65, stars: 0.75 wt %). The values in parentheses refer to the volume fraction of PLA particles, resulting from different volume ratios of aqueous XG with 15 wt % PLA in the formulations. See Table 1 for the decoding of the acronyms in the legend. Error bars are calculated as standard deviation (eq 8).

is larger than the latter, indicating a gel-like behavior. The difference between the two moduli increases with the content of XG when mixtures of comparable PLA content are considered, a clear indication of the key role of XG in inducing such gel-like behavior. At larger deformations, the storage modulus decreases at all investigated compositions, the onset of the deviation from the plateau occurring at progressively higher deformations with an increasing XG amount in the formulation. The inability of the system to completely recover the deformation within the experiment time frame corresponds to the typical behavior of solutions of high molecular weight polymers such as XG.[42] The loss moduli show a behavior similar to the storage moduli in the high-amplitude region at a low XG content. On the contrary, at a high XG content, a distinct peak is generally observed before the value starts decreasing, disclosing the presence of the so-called "weak strain overshoot". This behavior is typical of metastable complex fluids such as XG and it has been correlated to a decrease of the structural relaxation time at large strain values.[43,44]

The deviation from the plateau starts at lower deformation for the most concentrated solutions and it is faster for the storage than the loss moduli so that the two plots cross. The crossing point shifts at higher deformation for higher XG content, an indication that the system is able to dissipate progressively more energy and to recover elastically larger deformations when the concentration of xanthan gum increases. As a result, the linear viscoelastic region (LVR) becomes more extended, and the crossing point between storage and loss moduli shifts at higher strain as the concentration of XG increases.[42]

The frequency dependence of the viscoelastic moduli at constant strain in the 0.5−1% range for dispersions with different XG contents shows an increase of both storage and loss moduli with both increasing concentration and increasing frequency (Figure 6). The times of the experiment are too long

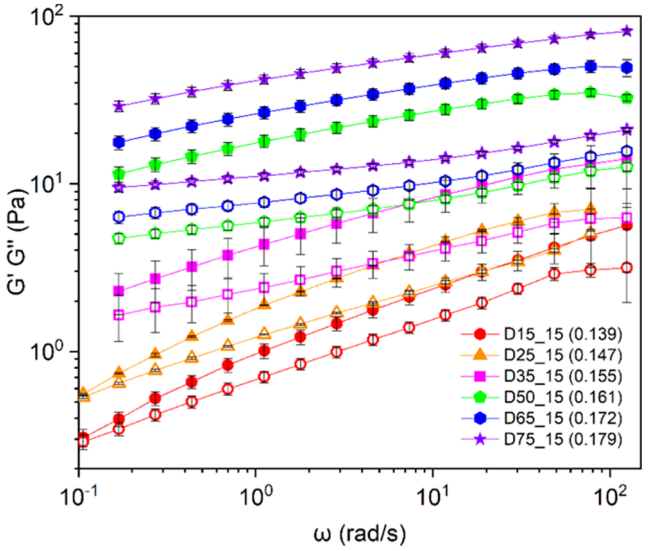

Figure 6. Storage (G'—full symbols) and loss (G—empty symbols) moduli as a function of frequency for dispersions with 15 wt % PLA particles and different XG concentrations (circles: 0.15, triangles: 0.25, squares: 0.35, pentagons: 0.50, hexagons: 0.65, stars: 0.75 wt %). The values in parentheses in the legend refer to the volume fraction of PLA particles, resulting from different volume ratios of aqueous XG with 15 wt % PLA in the formulations. See Table 1 for the decoding of the acronyms in the legend. Error bars are calculated as standard deviation (eq 8).

to allow the system to relax; therefore, the crossover frequency can hardly be observed and only at the lower investigated concentrations. As a result, the systems exhibit a solid-like behavior throughout the investigated frequency range ($G'' > G'$).

The plots of oscillatory shear flow experiments on samples with a comparable XG concentration showed an increase of the moduli values with increasing PLA concentration in the 5−20 wt % range (Figure 7). In addition, higher moduli are shown by samples with PLA particles as compared to samples without PLA particles (Figures 7 vs S5) at comparable XG concentrations. This behavior indicates that not only XG but also the dispersed PLA particles contribute to the viscoelasticity of the system. Indeed, both storage and loss moduli vs. frequency plots exhibit values dependent on both PLA and XG contents. In other words, even if the neat PLA dispersion does not exhibit any elastic behavior, we can say that PLA particles enhance both elastic and viscous behavior of the thickened dispersion, in a similar way that XG does (Figure 7).

https://doi.org/10.1021/acsomega.1c05382
ACS Omega 2022, 7, 12536−12548

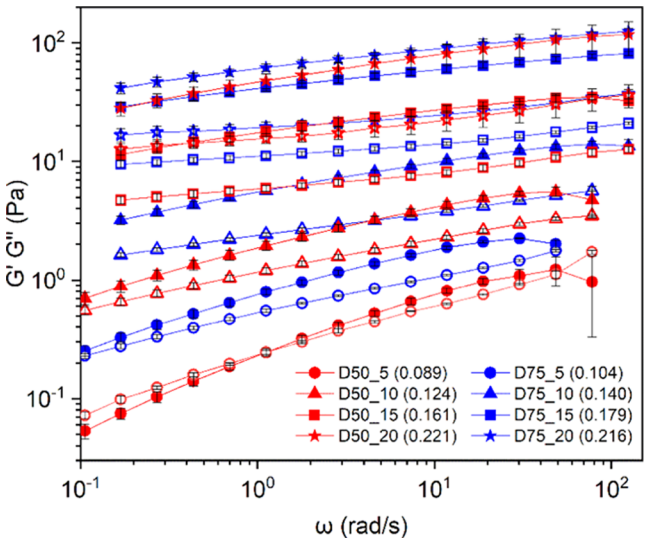

Figure 7. Storage (G'—full symbols) and loss (G''—empty symbols) moduli as a function of frequency for dispersions with different particle concentrations and fixed XG concentration (red symbols: 0.50%, blue symbols: 0.75 wt %). The values in parentheses in the legend refer to the volume fraction of PLA particles in the samples. See Table 1 for the decoding of the acronyms in the legend. Error bars are calculated as standard deviation (eq 8).

Therefore, the combined effects induced by the increase of both XG and dispersion particle concentrations result in a more pronounced viscoelastic behavior. The frequency dependence of the moduli is higher in the low concentration range; thus, the sample with the lowest concentrations of both PLA (5 wt %) and XG (0.5 wt %) is also the one displaying the crossover at the lowest frequency of about 1 rad/s, corresponding to a relaxation time of 5.5 s, indicative of a fluid-like behavior at low shear. None of the other samples presents the crossover within the investigated frequency range, indicating a more marked elastic behavior.

3. DISCUSSION

3.1. Volume Fraction. A critical discussion of the rheological behavior of the PLA dispersions described so far requires a clear understanding of the specific features of the system we are dealing with. The dispersed particles are made of amorphous PLA and its T_g = 54 °C was quite higher than the temperature at which the investigation was performed (25 °C). As a result, under the study conditions, the system can be approximated to a dispersion of hard spheres. The presence of SDS as the surfactant provides a negative surface charge to the particles, while XG in the continuous phase contributes to the negative charge of the mixed PLA/XG network and to the viscoelastic properties of the overall dispersion.[45] Therefore, we can describe the neat PLA dispersion as negatively charged hard spheres dispersed in a continuous liquid phase, and the PLA/XG system as negatively charged hard spheres dispersed in a complex anionic fluid matrix.[46] The rheological results described so far indicate that the viscoelasticity of the dispersion with XG arises from the presence of the polysaccharide in the continuous phase, as it generally occurs for dispersions of solid particles in polymeric matrices.[45] However, even if dispersions of neat PLA (hard) particles do not exhibit any viscoelasticity, the same particles do affect the viscoelastic response of the overall system once dispersed in a polymeric XG solution. Therefore, both components must be considered at once for a comprehensive discussion of the system behavior.

A single parameter including both components may be the particle volume fraction, Φ, defined as the fraction of volume occupied by the particles, Φ_i, with respect to the whole volume of the system, Φ_{TOT}. It depends on the number of particles n in the system and on the volume occupied by a single particle V_P, with respect to the total volume of the system (eq 1)

$$\Phi = \frac{\Phi_i}{\Phi_{TOT}} = \frac{n\,V_P}{V_{TOT}} \tag{1}$$

The total number of particles in dispersion is given by

$$n = \left(V_{TOT} - \frac{w_x}{\rho_x}\right) * V_P^{-1} = \left[V_{TOT} + \frac{(w_{dry} - w_{TOT})}{\rho_x}\right] * V_P^{-1} \tag{2}$$

where w_x is the weight of the solvent, w_{TOT} is the total weight of the sample, w_{dry} is the weight of the sample without the solvent, and ρ_x is the density of the solvent. By substituting eqs 2 in 1 and rearranging the equation for the volume fraction, eq 3 is obtained

$$\Phi = 1 + \frac{\rho_0}{\rho_x}\left(\frac{w_{dry}}{w_{TOT}} - 1\right) \tag{3}$$

where ρ_0 is the density of the dispersion.

In our study, ρ_0 and w_{dry}/w_{TOT} were assumed as equivalent to the density and the dry residue, respectively, of the neat PLA dispersions in water, irrespective of the presence and concentration of XG, while ρ_x was assumed as equivalent to the density of the XG solution at a given concentration in the absence of the dispersed particles. The volume fraction, Φ, was thus obtained by substituting in eq 3 the experimentally determined values for the densities (Figure S6) and the dry residues. The obtained values for the dispersions were found to depend on the concentrations of both PLA particles (C_P) and XG (C_X) (Figure 8). Hence, Φ can be used to describe the effects of the dispersion composition on the dispersion properties.

The calculated Φ values range between 0.09 and 0.22, scaling linearly with both PLA and XG concentrations, as indicated by the R^2 values larger than 0.9 for the linear fits of the data plots (Tables S1 and S4 in the supporting info).

Based on the new scale by the volume fraction, it is interesting to notice that the moduli vs. frequency plots shown in Figure 7 scale monotonically although the compositions differ in both PLA and XG concentrations. Indeed, if the storage, loss, and complex moduli at a fixed frequency (0.169 rad/s) are plotted as a function of the volume fraction in the log−log scale (Figure 9), an apparent linear trend is observed. This suggests that the amount of PLA particles in the dispersion affects its viscoelasticity by affecting the degree of crowding, intended as the total amount of species in the system, including the XG chains and the colloidal particles. Based on DLS analysis, XG does not adsorb irreversibly at the particle surface. In fact, in such a case, even after dilution, particles would be larger in the presence of XG than in its absence. Therefore, the observed effect must be ascribed to the presence of obstacles hindering the diffusion of the XG chains; such obstacles may consist solely of the PLA particles, although a contribution from weak van der Waals interactions or

https://doi.org/10.1021/acsomega.1c05382
ACS Omega 2022, 7, 12536−12548

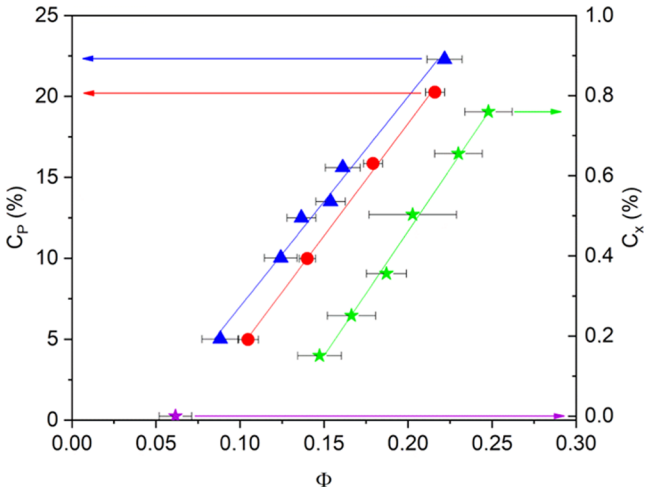

Figure 8. Left scale: volume fraction Φ of dispersions with different mass concentrations of particles, C_P, at a fixed XG concentration of 0.50 wt % (blue triangles; D50_5-20, Table 1) and 0.75 wt % (red dots; D75_5-20, Table 1), respectively. Right scale: volume fraction Φ of dispersions with different mass concentrations of XG, C_X, and fixed concentration of particles (green stars; D15-75_15, Table 1); violet star: volume fraction of the dispersion without XG and 15 wt % of particles (D0_15, Table 1). Straight lines: linear fitting (see Table S4 for fitting data). Error bars are calculated as standard deviation (eq 8).

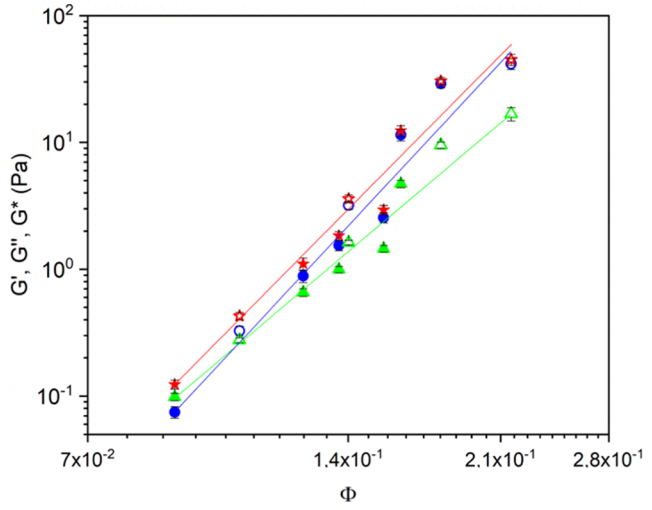

Figure 9. Complex (red stars), storage (blue circles), and loss (green triangles) moduli at 0.169 rad/s as a function of the volume fraction for dispersions with different particle concentrations and fixed XG concentration (full symbols: 0.50%, empty symbols: 0.75 wt %) (D50_5-20 and D75_5-20, Table 1). Straight lines are a guide to the eye.

scattered hydrogen bonds between PLA particles and XG chains, which are negligible at a low concentration but become relevant as the concentration increases, cannot be excluded.[47]

3.2. Master Curves of the Viscoelastic Moduli. The abovementioned direct increase of the viscoelastic moduli with the volume fraction suggests the possibility to build a master curve through the TCS concept (Figure 9).[42] To this purpose, at first, the data of the dispersions with 0.50 wt % of XG (D50_5-20) were elaborated. In particular, the data at 0.089 volume fraction were chosen as the reference, and the horizontal factors a_Φ for the different compositions were identified by shifting the loss factor tan δ (G''/G') onto the reference (Figure 10), according to the procedure described by

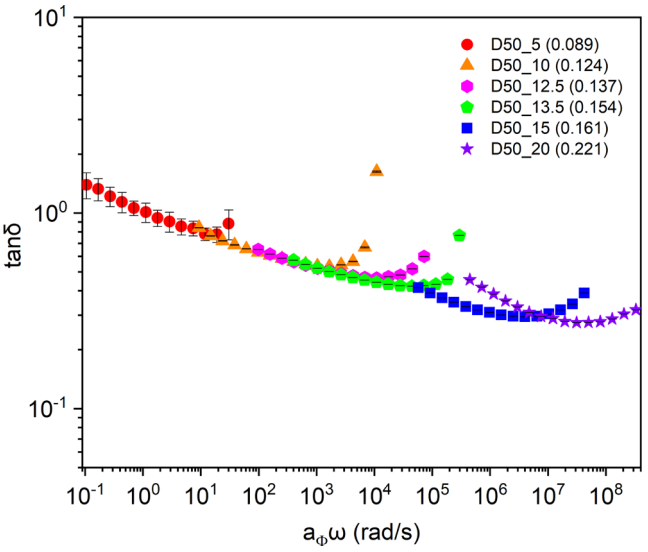

Figure 10. Master curve of the loss factor, tan δ, as a function of the scaled frequency, $\alpha_\Phi\omega$, for dispersions with different particle concentrations (C_P) and 0.50 wt % XG. The values in parentheses in the legend refer to the volume fraction of the samples. See Table 1 for the decoding of the acronyms in the legend. Error bars are calculated as standard deviation (eq 8).

McKenna and co-workers.[27] Similar to the procedure reported in the cited reference, the superposition of the plots of tan δ vs the scaled frequency, $\alpha_\Phi\omega$, is good for all the less concentrated samples (up to $\Phi = 0.154$) at all frequencies except at the highest ones. On the contrary, for the samples with higher concentrations ($\Phi \geq 0.161$), the superposition is poor even at low frequencies. This last deviation can be ascribed to the occurrence of a simultaneous β-relaxation process, as it will be discussed later.[27] Nevertheless, the horizontal shift factors determined through this procedure were applied to build the master curve of the complex modulus, G^*, throughout the range of investigated frequencies (Figure 11). To collapse the values of G^* of samples characterized by different volume fractions, the plots were shifted vertically, and such shifting procedure resulted in a newly calculated vertical complex shift factor, b^*_Φ. As a result, all plots of samples D50_x perfectly superimposed one another, except for those from the samples with the highest PLA content.

The same procedure was applied to all of the plots of PLA/XG samples with 0.75 wt % XG, resulting in a single master curve of the scaled complex modulus ($b_\Phi G^*$) as a function of the scaled frequency ($a_\Phi\omega$) for samples with 0.50% and 0.75 wt % XG (Figure 14). In the case of 0.75 wt % XG samples, the plots at the highest PLA concentrations showed poorer superposition as in the case of the lowest XG concentration. In any case, the obtained master curve included most of the characterized samples with good accuracy, thus demonstrating that the crowding of the system is the only factor that matters for the investigated PLA/XG system. In other words, the effect of PLA particles is only one of reducing the available volume for XG to diffuse, a similar effect resulting from an increase of the XG concentration.

The a_Φ and b_Φ factors used to build the master curve for the complex modulus were also successfully used to obtain the

https://doi.org/10.1021/acsomega.1c05382
ACS Omega 2022, 7, 12536−12548

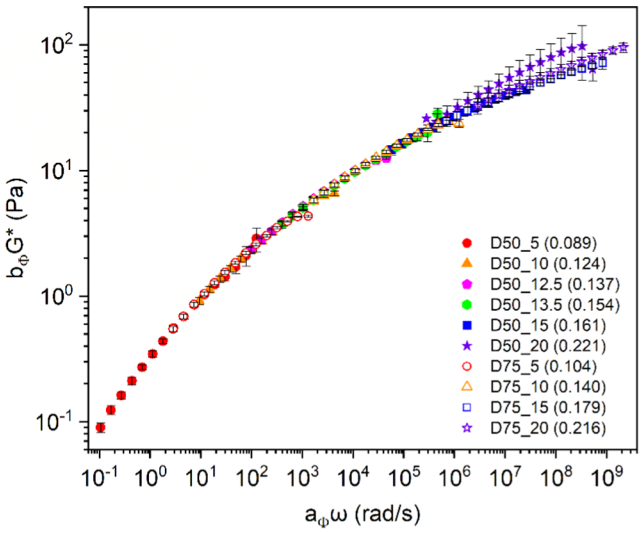

Figure 11. Master curve of the scaled complex modulus as a function of the scaled frequency, for dispersions with different particle concentrations (C_P) and fixed XG concentrations of 0.50 (full symbols) and 0.75 wt % (empty symbols), respectively. The values in parentheses in the legend refer to the volume fraction of the samples. See Table 1 for the decoding of the acronyms in the legend. Error bars are calculated as standard deviation (eq 8).

corresponding plots for the real and imaginary parts of G^* (Figure 12).

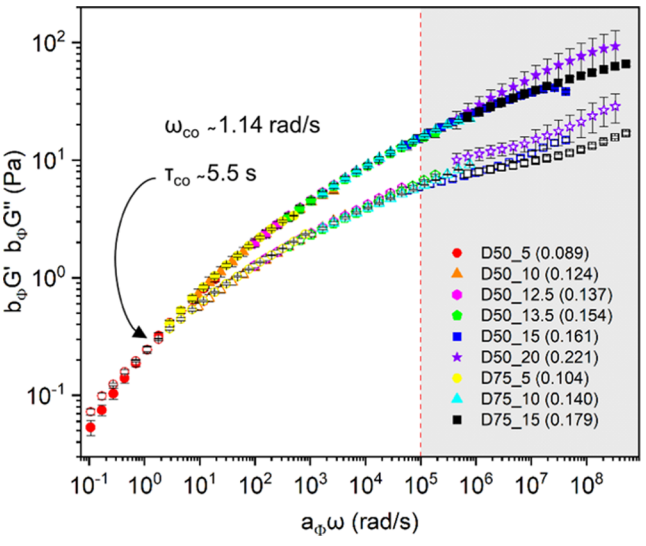

Figure 12. Master curve of the scaled storage (full symbols) and loss (empty symbols) moduli as a function of the scaled frequency for dispersions with different particle concentrations (C_P) and fixed XG concentrations of 0.50 (red, orange, magenta, green, blue, and violet symbols) and 0.75 wt % (yellow, cyan, black symbols). The values in parentheses in the legend refer to the volume fraction of the samples. See Table 1 for the decoding of the acronyms in the legend. Error bars are calculated as standard deviation (eq 8).

Nevertheless, a deviation from the master curve was observed for the highest PLA concentrations, in particular for the loss factor. The inconsistency is here even more evident than for the complex viscoelastic moduli. As mentioned for tan δ, a similar deviation was reported by McKenna and co-workers and was attributed to the presence of β-relaxation,[27] a process typically activated at higher frequencies than α-relaxation. Götze[48] described the β-relaxation process in colloidal systems through a cage effect. In a concentrated system, at any instant, a particle is surrounded by a shell of nearest neighbors (the cage). These cages represent metastable states with a partially arrested structure, which can display a very long lifetime. For volume fractions below the highest random close packing, the β-process describes the motion where the cages are almost but not yet completely closed. However, the range of volume fractions investigated by us lies quite below the value characteristic of random close packing. Therefore, the observed relaxation could well be ascribed to the polysaccharide chains. Indeed, the presence of several relaxation modes in mono-, di-, and polysaccharides was evidenced by dielectric spectroscopy.[49,50] In sucrose, this relaxation was associated with a twisting rotation of the two monosugar rings (glucose and fructose) around the glycosidic bond.[51−53] Something similar may also occur in XG.

Irrespective of the origin of the β-process, the coexistence and the overlap of the two relaxation processes do not comply with the TCS concept, and thus, it is not possible to extend the master curve over the frequency range where the superposition occurs ($\omega > 10^5$ rad/s).[29] In any case, the master curves obtained through the TCS concept allowed us to predict the behavior of PLA/XG samples with $\Phi = 0.089$ in the 0.1−100 000 rad/s frequency range, which is broader than the ones experimentally accessible, namely 0.1−200 rad/s. In the extended frequency window, the system shows both a fluidlike behavior at low frequencies and a weak gel one at high frequencies with a characteristic relaxation time, τ_{co}, of 5.5 s (Figure 12).

3.3. Viscosity Master Curve. The shift factors used to build the master curve of the moduli were also used to build the master curve for the complex viscosity via eq 4

$$\eta^*(\Phi, \omega) = \frac{b_\Phi}{a_\Phi}\eta^*(\Phi, a_\Phi\omega) \tag{4}$$

The obtained master curve represents the scaled complex viscosity ($a_\Phi/b_\Phi\eta^*$) as a function of the scaled frequency ($a_\Phi\omega$) (Figure 13). It operates even at the highest XG concentrations, where the moduli-based master curve failed, namely for $\Phi > 0.161$. In fact, in this case, the plots superimposed quite well after the shifting operation. However, the obtained master curve of η^* could not be adequately described with the Carreau−Yasuda model (eq 5) at a frequency >10^5 rad/s (Figure 13, inset), where the α- and β-relaxation processes coexist. On the contrary, the model describes quite well the data in the lower frequency region.

$$\eta^* = \eta_\infty + (\eta_0 - \eta_\infty)\cdot[1 + (\tau\omega)^a]^{(n-1)/a} \tag{5}$$

In the Carreau−Yasuda model (eq 5), the parameters η_∞ and η_0 represent the asymptotic values of the viscosity at infinite and 0 frequency, respectively, τ is the relaxation time, a is a constitutive parameter, and n is the flow index. The relaxation time (also called the characteristic time) of the system, calculated from the fitting of the master curve, was $\tau = 13.3$ s, in the same range as the one obtained from the crossover frequency τ_{co} of the master curve of the viscoelastic moduli.

3.4. Shift Parameters. The dependence of the shift factors a_Φ and b_Φ on the volume fraction (Figure 14) is often described by the Vogel−Fulcher−Tammann (VFT) equation[27]

https://doi.org/10.1021/acsomega.1c05382
ACS Omega 2022, 7, 12536−12548

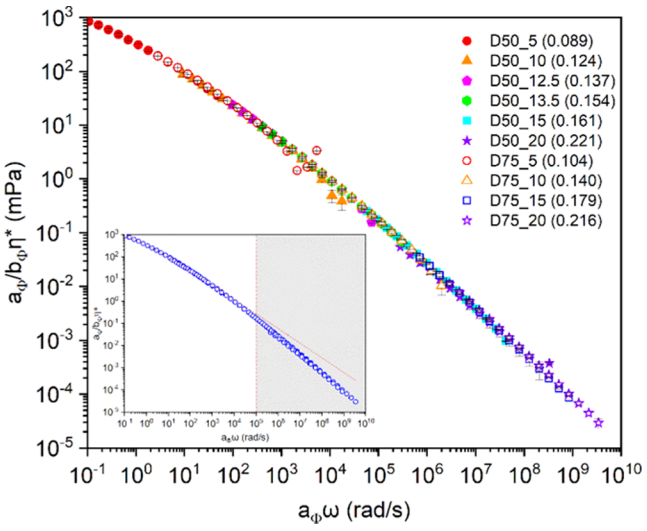

Figure 13. Master curve of the scaled complex viscosity as a function of the scaled frequency for dispersions with different particle concentrations (C_p) and fixed XG concentrations 0.50 (full symbols) and 0.75 wt %. (empty symbols). The values in parentheses in the legend refer to the volume fraction of the samples. The inset shows the fitting of the master curve of the complex viscosity. Red curve: fitting (see Table S5 for fitting data). See Table 1 for the decoding of the acronyms in the legend. Error bars are calculated as standard deviation (eq 8).

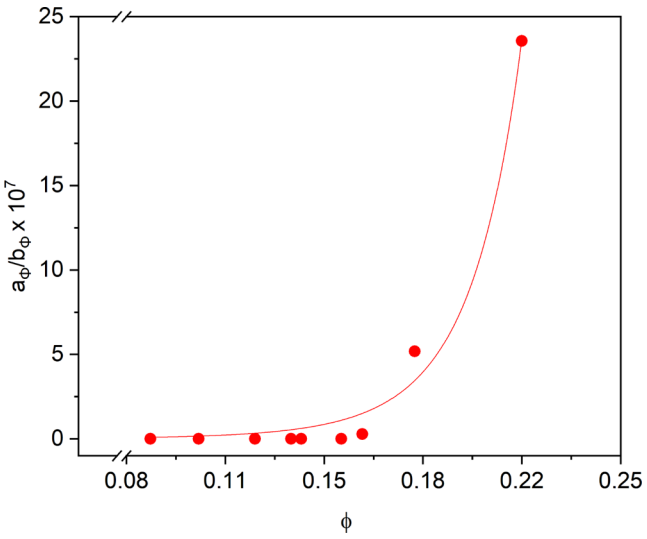

Figure 14. Ratio of the shift factors (red dots) as a function of the volume fraction; the red curve represents the VFT fit. See Table S6 for fitting data.

$$\log \frac{a_\Phi}{b_\Phi} = A + \frac{B}{\Phi - \Phi_\infty} \quad (6)$$

where A and B are the VFT parameters and Φ_∞ represents the volume fraction at which the motion of the particles freezes completely (random close packing).

The best fit of the experimental data provides a value of volume fraction at random close packing, $\Phi_\infty = 0.62 \pm 0.02$. Despite the poor interpolation of the experimental data by the adopted model (Figure 14), it is surprising that the obtained Φ_∞ value is similar to those determined both theoretically and experimentally for hard-sphere dispersions.[46,54]

4. CONCLUSIONS

In the present study, aqueous PLA dispersions targeting coating applications were prepared and thickened by the addition of xanthan gum (XG). The colloidally stable neat PLA dispersion, consisting of negatively charged particles of 222 ± 2 nm size, was found to remain stable over time irrespective of the presence of XG, thus indicating the suitability of XG as a thickener for this system. The results of the rheological analysis performed in steady and oscillatory conditions on dispersions with the PLA content ranging between 5 and 22 wt % and XG between 0 and 0.76 wt % showed a transition from the very low viscosity of the neat PLA dispersions, typical of diluted colloids, to the honey-like viscosity and strong viscoelastic behavior of the dispersions obtained upon the addition of XG, even at low concentrations. All of the investigated PLA/XG formulations showed a gel-like behavior throughout the explored frequency range, with the exception of the most diluted sample (PLA 5 wt %), which revealed a fluid character before the crossover frequency. Both storage and loss moduli of PLA/XG samples vary monotonically with the concentration of either PLA particles or XG, thus indicating the participation of both components in the gel network. The applicability of the TCS concept to the studied system, by superimposing viscoelastic curves of dispersions at two different concentrations of XG and six concentrations of PLA particles, was also demonstrated. This allowed achieving a description of the dynamics of these dispersions over a range of relaxation times greater than that accessible by direct measurements. The TCS concept failed at 10^5 rad/s, revealing the onset of β-relaxation modes, overlapped to α-relaxation. The understanding and control of the rheological properties of the PLA/XG formulations achieved in this study is an important starting point to explore the potential for different applications of these colloidal dispersions. Indeed, thanks to the advantages that PLA inherently offers (bio-based, stability, nontoxicity, food compliance) and to the interesting properties of the formulations described here, the range of possible applications could span from coatings for paper-based food packaging and single-use compostable items to component for indoor paints.[7] Finally, the obtained results suggest a high potential for XG to be exploited in new application fields.

5. EXPERIMENTAL SECTION

5.1. Materials. Polylactic acid Ingeo PLA 4060D (PLA) was supplied by NatureWorks LLC (Minetonka, MN). PLA 4060D is an amorphous polymer with an L-lactide content of around 88 wt % and a weight-average molecular weight $\bar{M}_w$ = 1.15 × 10^5 g/mol.[36] Sodium dodecyl sulfate (SDS, purity ≥99.0%) and ethyl acetate (purity ≥99.5%) were purchased from Sigma-Aldrich. Starch C*Icoat 07525 (starch) and xanthan gum Satiaxane CX 2 QD (XG) were provided by Cargill Deutschland GmbH.

5.2. Preparation of Water Dispersion of Polylactic Acid. A 3 wt % solution of starch in ultrapure water was prepared by heating at a reflux temperature for 1 h. About 51.8 g of this solution was diluted to 280 g with ultrapure water and then 2.24 g of SDS was added. Meanwhile, 40 g of PLA was solubilized in 360 mL of ethyl acetate under vigorous stirring for 4 h. After parting both the oil and the water phases each in 8 equal fractions, 8 equal mixtures were prepared by mixing one to one the oil and of the water phases, followed by homogenization and ultrasound treatment (Vibra-Cell Ultra-

https://doi.org/10.1021/acsomega.1c05382
ACS Omega 2022, 7, 12536−12548

sonic Liquid Processor VCX750, maximum power output: 750 W, equipped with a 13 mm diameter probe) in four continuous steps of 30 sec each. The power amplitude was 50% in the first step and then 90%. Steps were spaced out by 2 min during which the mixture was kept under mechanical stirring with an overhead stirrer. Each one of the resulting emulsions was separately collected in a 1 L reactor and the organic solvent, ethyl acetate, was distilled off at 40 °C and 0.85 bar for 4 h while keeping the emulsion under stirring at 120 rpm, resulting in a residual ethyl acetate content <40 ppm by GC analysis and dry matter content ≥15 wt % at 200 °C.

5.3. Preparation of Water Dispersion of Polylactic Acid with XG. Dispersions with PLA and XG contents in the 5−22 and 0.15−0.76 wt % range, respectively, were prepared (Table 1). They are identified with the acronym D*x*_*p*, where *x* stands for the concentration of XG given as 100× wt % and *p* for the wt % concentration of PLA in the final aqueous dispersions. Aqueous dispersions with 15 wt % PLA and different amounts of XG (0.15, 0.25, 0.35, 0.50, 0.65, and 0.75 wt %) were obtained from the pristine PLA dispersion by adding an appropriate amount of XG, stirring the mixture at 200 rpm overnight at room temperature, and then keeping the dispersion under mild vacuum until air bubbles were removed.

Dispersions with concentrations of PLA particles lower than 15 wt % (5, 10, 12.5, and 13.5 wt %, respectively) were obtained by diluting the pristine PLA dispersion with ultrapure water before the addition of XG. Dispersions with 20 wt % PLA were obtained by processing the 15 wt % dispersion through an ultrafiltration cell (Millipore Amicon 8003) equipped with a 100 kDa (membrane filter Ultracel 100 kDa Millipore) until the desired concentration of particles was reached (few minutes). Two dispersions were obtained by thickening with XG at 0.50 and 0.75 wt %, respectively. Reference XG aqueous solutions at 0.15, 0.25, 0.50, and 0.75 wt % were prepared by stirring a suitable amount of the thickening agent in ultrapure water for a couple of hours.

5.4. Instruments and Methods. The dry residue (C_P) of each dispersion was determined by drying 250 mg (w_{TOT}) of the sample in an oven at 200 °C for 20 min, followed by weighing (w_{dry})

$$C_P = \frac{w_{dry}}{w_{TOT}} \times 100 \tag{7}$$

The diameter of the particles was determined by dynamic light scattering (DLS) analysis at 25 °C using a NanoBrook Omni Particle Size Analyzer (Brookhaven Instruments Corporation) equipped with a 35 mW red diode laser (nominal 640 nm wavelength). Samples at 0.15 wt % were analyzed by setting the refractive index of the dispersion medium and of the dispersed phase at 1.330 and 1.596, respectively. Each measurement was repeated five times on the same sample, and the reported data were the average over the five measurements. The error was calculated as standard deviation, σ (eq 8)

$$\sigma = \frac{1}{\sqrt{N-1}} \sum_{i=1}^{N} \sqrt{(x_i - \bar{x})^2} \tag{8}$$

where N is the number of measurements, x_i is the value of the ith measurement, and $\bar{x}$ is the arithmetic mean.

The Z-potential of the dispersions was determined by phase analysis light scattering (PALS) at 25 °C using a NanoBrook Omni Particle Size Analyzer (Brookhaven Instruments Corporation) equipped with a 35 mW red diode laser (nominal 640 nm wavelength). The analyses were carried out on samples at 0.25 wt %, and the reported data are the average over five repeated measurements.

Size-exclusion chromatography (SEC) analyses were performed with a Jasco (Jasco Europe SRL, Cremella, Italy) instrument comprising a PU-2089 Plus quaternary pump and injector with a 20 μL loop, two in series PLgel MIXED-D columns (Agilent Technologies Italia S.p.A., Cernusco sul Naviglio, Italy; linearity range 200 to 2 000 000 g/mol based on polystyrene equivalent) placed in a Jasco CO-2065 column oven set at 30 °C, a Jasco RI-2031 Plus refractive index detector, and a Jasco UV-2077 Plus multichannel UV-Vis detector. The sample in the form of films or powders was dissolved in trichloromethane (HPLC grade Sigma-Aldrich) with the aid of sonication and filtered through a 0.2 μL pore size PTFE filter to remove the insoluble fraction before injection as a 5 mg/mL solution; elution was performed with trichloromethane at 1 mL/min flow rate. ChromNav Jasco software was used for data acquisition and analysis; the weight-average ($\bar{M}_w$) and number-average ($\bar{M}_n$) molecular weights are based on a calibration curve obtained by running a set of four monodisperse polystyrene standards (19 000, 50 000, 233 000, and 300 000 g/mol, respectively) and performing a fourth-order fit.

A Zeiss LEO 1530 scanning electron microscope equipped with a field emission gun as an ionization source was employed for the morphological analysis of the dried formulations. Samples obtained by air drying 1 mL of dispersion in Petri dishes at room temperature were sputtered with gold before observation.

Differential scanning calorimetry (DSC) analysis was performed on a DSC 8000 (PerkinElmer Inc.) instrument equipped with an IntraCooler II cooling device and Pyris V13.3 software for instrument control, data acquisition, and analysis. The instrument was calibrated for temperature and energy with indium and zinc standards. About 5−10 mg of dry samples were analyzed in aluminum pans under a dry nitrogen atmosphere (30 mL min^{-1}). Samples were heated up from 25 to 200 °C to erase the thermal history and to remove any trapped volatile substances such as residual solvent; then, they were cooled to −70 °C (cooling step), maintained at −70 °C for 5 min, and finally, heated up again to 200 °C (second heating step). Both heating and cooling steps were performed at 10 °C min^{-1}. Thermogravimetric analysis (TGA) was carried out on a TGA 4000, (PerkinElmer Inc.) instrument with Pyris software for data acquisition and analysis. Samples (5−10 mg) were analyzed in an alumina pan at a heating rate of 10 °C min^{-1} from 30 to 720 °C under a nitrogen atmosphere (30 mL min^{-1}).

The densities of the emulsions and solutions were determined by measuring the weight of a precise volume of sample (2−5 mL) in a controlled temperature system. Each measure was repeated ten times, and the data were taken as an arithmetic average value on the calculated density. Data error was calculated as standard deviation.

The rheology measurements were performed with an Anton Paar MCR 102 Rheometer, equipped with a cone-plate CP50-1 (49 975 mm of diameter) probe and Anton Paar software for data acquisition and analysis. A solvent reservoir was attached to prevent the sample from drying. Steady shear experiments were performed at 25 °C by recording the flow curves in the range of shear rates from 1 to 1000 s^{-1}. Such experiments were

https://doi.org/10.1021/acsomega.1c05382
ACS Omega 2022, 7, 12536−12548

possible because weak xanthan gum gels do not exhibit rupture or edge fracture even at large deformations.[55] Each measurement on a given sample was repeated at least three times, and the arithmetic mean was calculated on the collected data. The error was calculated as standard deviation. Before each oscillatory measurement, a preshear at 100 s^{-1} for 60 s followed by a 300 s rest was applied to erase the effect of loading. Amplitude oscillatory sweep tests were performed to determine the linear viscoelastic range (LVR), and the viscoelastic response in the strain range from 0.01 to 200% was measured at ω = 1 rad s^{-1}. Frequency sweep tests were performed at a strain amplitude within the previously determined linear viscoelasticity range. Each measurement on a given sample was repeated at least three times, and the arithmetic mean was calculated on the collected data. The error on the viscoelastic moduli was calculated as standard deviation. Further elaboration of the collected data was performed with OriginPro 2018 software.

■ ASSOCIATED CONTENT

Supporting Information

The Supporting Information is available free of charge at https://pubs.acs.org/doi/10.1021/acsomega.1c05382.

Calculated volume fraction Φ, mean diameter ⟨d⟩, polydispersity (IPD), and viscosity η at a shear rate 1 s^{-1} for all prepared dispersions of PLA/xanthan gum (XG); Z potential, mobility, and conductance of PLA dispersions without XG. TGA, DSC, and GPC analyses of the dried PLA dispersion; SEM images of the dried PLA dispersion with and without XG. Viscosity plots of xanthan gum solutions at different concentrations and comparison between the viscosity curves of xanthan gum solutions with and without PLA particles; density of the prepared PLA/XG dispersions as a function of the PLA and XG contents; best-fitting parameters for (1) the dependence of the volume fraction on sample's composition (Figure 8), (2) dependence of the scaled complex viscosity, η^*, on the scaled frequency, ω, and (3) dependence of the shift factors on the volume fraction Φ (PDF)

■ AUTHOR INFORMATION

Corresponding Author

Monica Bertoldo − *Department of Chemical, Pharmaceutical and Agricultural Sciences, University of Ferrara, Ferrara 44121, Italy; Institute of Organic Synthesis and Photoreactivity−Italian National Research Council, Bologna 40129, Italy;* orcid.org/0000-0002-8221-2095; Email: monica.bertoldo@unife.it

Authors

Sara Buoso − *Institute of Organic Synthesis and Photoreactivity−Italian National Research Council, Bologna 40129, Italy*

Giada Belletti − *Department of Chemical, Pharmaceutical and Agricultural Sciences, University of Ferrara, Ferrara 44121, Italy; Institute of Organic Synthesis and Photoreactivity−Italian National Research Council, Bologna 40129, Italy*

Daniele Ragno − *Department of Chemical, Pharmaceutical and Agricultural Sciences, University of Ferrara, Ferrara 44121, Italy;* orcid.org/0000-0003-0016-290X

Valter Castelvetro − *Department of Chemistry and Industrial Chemistry, University of Pisa, Pisa 56124, Italy;* orcid.org/0000-0002-3302-7037

Complete contact information is available at: https://pubs.acs.org/10.1021/acsomega.1c05382

Notes

The authors declare no competing financial interest.

■ ACKNOWLEDGMENTS

This research was supported by the Bio-Based Industries Joint Undertaking under the European Union Horizon 2020 research program (BBI-H2020), Sherpack, Innovative structured polysaccharides-based materials for recyclable and biodegradable flexible packaging, GA745718.

■ REFERENCES

(1) Nagarajan, V.; Mohanty, A. K.; Misra, M. Perspective on Polylactic Acid (PLA) based Sustainable Materials for Durable Applications: Focus on Toughness and Heat Resistance. *ACS Sustainable Chem. Eng.* **2016**, *4*, 2899−2916.

(2) Nofar, M.; Sacligil, D.; Carreau, P. J.; Kamal, M. R.; Heuzey, M.-C. Poly (lactic acid) blends: Processing, properties and applications. *Int. J. Biol. Macromol.* **2019**, *125*, 307−360.

(3) Nasrin, R.; Biswas, S.; Rashid, T. U.; Afrin, S.; Jahan, R. A.; Haque, P.; Rahman, M. M. Preparation of Chitin-PLA laminated composite for implantable application. *Bioact. Mater.* **2017**, *2*, 199−207.

(4) (a) Allemann, E.; Doelker, E.; Fessi, H.; Gurny, R.; Quintanar-Guerrero, D. Method for producing an aqueous colloidal dispersion of nanoparticles. WO99/335581997. (b) Mentink, R. L.; Bouvier, L. F.; Clabaux, G. P.-P.; Bernaerts, L. J. Use of an aqueous dispersion of at least one biodegradable polymer containing at least one stabilizing agent for the preparation of an aqueous filmogenic composition. U.S. Patent US2007/0088099 A12007.

(5) Bertoldo, M.; Ricci, L.; Messina, T.; Belletti, G.; Blanca, M. G.; Ortiz, A. G.; Gutierrez, A. A. Halogen-free aqueous dispersions of biodegradable polymers and process for preparing the same (dispersioni acquose di polimeri biodegradabili prive di alogeni e procedimento per la loro preparazione). Italian Patent issue n., 1020200000286402020).

(6) (a) Ferrández-Montero, A.; Lieblich, M.; Benavente, R.; González-Carrasco, J. L.; Ferrari, B. Study of the matrix-filler interface in PLA/Mg composites manufactured by Material Extrusion using a colloidal feedstock. *Addit. Manuf.* **2020**, *33*, No. 101142. (b) Ferrandez-Montero, A.; Lieblich, M.; Benavente, R.; González-Carrasco, J. L.; Ferrari, B. New approach to improve polymer-Mg interface in biodegradable PLA/Mg composites through particle surface modification. *Surf. Coat. Technol.* **2020**, *383*, No. 125285. (c) Yu, B.; Zhao, Z.; Fu, S.; Meng, L.; Liu, Y.; Chen, F.; Wang, K.; Fu, Q. Fabrication of PLA/CNC/CNT conductive composites for high electromagnetic interference shielding based on Pickering emulsions method. *Composites, Part A* **2019**, *125*, No. 105558. (d) Ribeiro, H. S.; Chu, B.-S.; Ichikawa, S.; Nakajima, M. Preparation of nanodispersions containing β-carotene by solvent displacement method. *Food Hydrocolloids* **2008**, *22*, 12−17. (e) Assunção, L. S.; Bezerra, P. Q. M.; Poletto, V. S. H.; Rios, A. O.; Ramos, I. G.; Ribeiro, C. D. F.; Machado, B. A. S.; Druzian, J. I.; Costa, J. A. V.; Nunes, I. L. Combination of carotenoids from Spirulina and PLA/PLGA or PHB: New options to obtain bioactive nanoparticles. *Food Chem.* **2021**, *346*, No. 128742. (f) Machado, M. G. C.; Pound-Lana, G.; Oliveira, M. A.; Lanna, E. G.; Fialho, M. C. P.; Brito, A. C. F.; Barboza, A. P. M.; Oliveira Aguiar-Soares, R. D.; Mosqueira, F. C. F. PLA-PEG nanocarriers with IR780: physical entrapment versus covalent attachment to polylactide. *Drug Delivery Transl. Res.* **2020**, *10*, 1626−1643.

(7) Belletti, G.; Buoso, S.; Ricci, L.; Ortiz, A. G.; Gutiérrez, A. A.; Bortolini, O.; Bertoldo, M. Preparations of polylactic acid dispersions in water for coating applications. *Polymers* **2021**, *13*, 2767.
(8) Eley, R. R. Applied rheology and architectural coating performance. *J. Coat. Technol. Res.* **2019**, *16*, 263−305.
(9) Rueda, M. M.; Auscher, M.-C.; Fulchiron, R.; Périé, T.; Martin, G.; Sonntag, P.; Cassagnau, P. Rheology and applications of highly filled polymers: A review of current understanding. *Prog. Polym. Sci.* **2017**, *66*, 22−53.
(10) Kästner, U. The impact of rheological modifiers on water-borne coatings. *Colloids Surf., A* **2001**, *183*−*185*, 805−821.
(11) Bhavsar, R. A.; Nehete, K. M. Rheological approach to select most suitable associative thickener for water-based polymer dispersions and paints. *J. Coat. Technol. Res.* **2019**, *16*, 1089−1098.
(12) Jansson, P.; Kenne, L.; Lindberg, B. Structure of the extracellular polysaccharide from xanthomonas campestris. *Carbohydr. Res.* **1975**, *45*, 275−282.
(13) Galván, Z. R. N.; Soares, L. S.; Medeiros, E. A. A.; Soares, N. F. F.; Ramos, A. M.; Coimbra, J. S. R.; Oliveira, E. B. Rheological Properties of Aqueous Dispersions of Xanthan Gum Containing Different Chloride Salts Are Impacted by both Sizes and Net Electric Charges of the Cations. *Food Biophys.* **2018**, *13*, 186−197.
(14) Petri, D. F. S. Xanthan gum: A versatile biopolymer for biomedical and technological applications. *J. Appl. Polym. Sci.* **2015**, *132*, No. 42035.
(15) Sara, H.; Yahoum, M. M.; Lefnaoui, S.; Abdelkader, H.; Moulai-Mostefa, N. New alkylated xanthan gum as amphiphilic derivatives: Synthesis, physicochemical and rheological studies. *J. Mol. Struct.* **2017**, *1207*, No. 127768.
(16) Wang, L.; Xiang, D.; Li, C.; Zhang, W.; Bai, X. Effects of lyophilization and low-temperature treatment on the properties and conformation of xanthan gum. *Food Hydrocolloids* **2021**, *112*, No. 106352.
(17) Ross-Murphy, S. B.; Morris, V. J.; Morris, E. R. Molecular viscoelasticity of xanthan polysaccharide. *Faraday Symp. Chem. Soc.* **1983**, *18*, 115−129.
(18) Rochefort, W. E.; Middleman, S. Rheology of Xanthan Gum: Salt, Temperature, and Strain Effects in Oscillatory and Steady Shear Experiments. *J. Rheol.* **1987**, *31*, 337−369.
(19) Saha, D.; Bhattacharya, S. Hydrocolloids as thickening and gelling agents in food: a critical review. *J. Food Sci. Technol.* **2010**, *47*, 587−597.
(20) (a) Lee, H.; Yoo, B. Agglomerated xanthan gum powder used as a food thickener: Effect of sugar binders on physical, microstructural, and rheological properties. *Powder Technol.* **2020**, *362*, 301−306. (b) Kim, H.; Hwang, H.-I.; Song, K.-W.; Lee, J. Sensory and rheological characteristics of thickened liquids differing concentrations of a xanthan gum-based thickener. *J. Texture Stud.* **2017**, *48*, 571−585.
(21) Yadav, K.; Yadav, B. S.; Yadav, R. B.; Dangi, N. Physicochemical, pasting and rheological properties of colocasia starch as influenced by the addition of guar gum and xanthan gum. *Food Measure.* **2018**, *12*, 2666−2676.
(22) Zhang, R.; Tao, Y.; Xu, Q.; Liu, N.; Chen, P.; Zhou, Y.; Bai, Z. Rheological and ion-conductive properties of injectable and self-healing hydrogels based on xanthan gum and silk fibroin. *Int. J. Biol. Macromol.* **2020**, *144*, 473−482.
(23) Cargill Icorporated website. https://www.cargill.com/bioindustrial/xanthan-gum (accessed June 24, 2021).
(24) (a) Llinares, R.; Ramírez, P.; Carmona, J. A.; Trujillo-Cayado, L. A.; Muñoz, J. Assessment of Fennel Oil Microfluidized Nanoemulsions Stabilization by Advanced Performance Xanthan Gum. *Foods* **2021**, *10*, 693. (b) Villada, Y.; Gallardo, F.; Erdmann, E.; Casis, N.; Olivares, L.; Estenoz, D. Functional characterization on colloidal suspensions containing xanthan gum (XGD) and polyanionic cellulose (PAC) used in drilling fluids for a shale formation. *Appl. Clay Sci.* **2017**, *149*, 59−66. (c) Muhammad, D. R. A.; Doost, A. S.; Gupta, V.; Sintang, M. D.; Walle, D. V.; Meeren, P. V.; Dewettinck, K. Stability and functionality of xanthan gum−shellac nanoparticles for the encapsulation of cinnamon bark extract. *Food Hydrocolloids* **2020**, *100*, No. 105377. (d) Martín-Alfonso, J. E.; Cuadri, A. A.; Berta, M.; Stading, M. Relation between concentration and shear-extensional rheology properties of xanthan and guar gum solutions. *Carbohydr. Polym.* **2018**, *181*, 63−70. (e) Desplanques, S.; Renou, F.; Grisel, M.; Malhiac, C. Impact of chemical composition of xanthan and acacia gums on the emulsification and stability of oil-in-water emulsions. *Food Hydrocolloids* **2012**, *27*, 401−410.
(25) Joshi, Y. M. Dynamics of Colloidal Glasses and Gels. *Annu. Rev. Chem. Biomol. Eng.* **2014**, *5*, 181−202.
(26) Ahmed, J. Time−Temperature Superposition Principle and its Application to Biopolymer and Food Rheology. *Advances in Food Rheology and Its Applications*; Woodhead Publishing, 2017; Chapter 9, pp 209−241.
(27) Sundaravadivelu Devarajan, D.; Nourian, P.; McKenna, G. B.; Khare, R. Molecular simulation of nanocolloid rheology: Viscosity, viscoelasticity, and time concentration superposition. *J. Rheol.* **2020**, *64*, 529−543.
(28) Trappe, V.; Weitz, D. A. Scaling of the Viscoelasticity of Weakly Attractive Particles. *Phys. Rev. Lett.* **2000**, *85*, 449−452.
(29) Peng, X.; Wang, J. G.; Li, Q.; Chen, D.; Zia, R. N.; McKenna; B, G. Exploring the validity of time-concentration superposition in glassy colloids: Experiments and simulations. *Phys. Rev. E* **2018**, *98*, No. 062602.
(30) Mattsson, J.; Wyss, H. M.; Fernandez-Nieves, A.; Miyazaki, K.; Hu, Z.; Reichman, D. R.; Weitz, D. A. Soft colloids make strong glasses. *Nature* **2009**, *462*, 83−86.
(31) Bae, J.-E.; Jung, J. B.; Kim, K.; Lee, S.-M.; Kang, N.-G. A study on time-concentration superposition of dilatational modulus and foaming behavior of sodium alkyl sulfate. *J. Colloid Interface Sci.* **2019**, *556*, 704−716.
(32) Wen, Y. H.; Schaefer, J. L.; Archer, L. A. Dynamics and Rheology of Soft Colloidal Glasses. *ACS Macro Letters* **2015**, *4*, 119−123.
(33) Wen, Y. H.; Lu, Y.; Dobosz, K. M.; Archer, L. A. Structure, Ion Transport, and Rheology of Nanoparticle Salts. *Macromolecules* **2014**, *47*, 4479−4492.
(34) Murariu, M.; Dubois, P. PLA composites: From production to properties. *Adv. Drug Delivery Rev.* **2016**, *107*, 17−46.
(35) Al-Itry, R.; Lamnawar, K.; Maazouz, A. Biopolymer Blends Based on Poly (lactic acid): Shear and Elongation Rheology/Structure/Blowing Process Relationships. *Polymers* **2015**, *7*, 939−962.
(36) Zhang, W.; Huang, C.; Kusmartseva, O.; Thomas, N. L.; Mele, E. Electrospinning of polylactic acid fibres containing tea tree and manuka oil. *React. Funct. Polym.* **2017**, *117*, 106−111.
(37) NatureWork processing guide NWPG002_020111, Crystallizing and Drying Ingeo Biopolymer. http://ifbb-knvb.wp.hs-hannover.de/db/files/downloads/ProcessingGuide_Crystallizing-and-Drying_pdf_1430990865.pdf (accessed June 25, 2021).
(38) Lim, L.-T.; Auras, R.; Rubino, M. Processing technologies for poly(lactic acid). *Prog. Polym. Sci.* **2008**, *33*, 820−852.
(39) Yu, L.; Christie, G. Measurement of starch thermal transitions using differential scanning calorimetry. *Carbohydr. Polym.* **2001**, *46*, 179−184.
(40) Laun, H. M. Rheological properties of aqueous polymer dispersions. *Angew. Makromol. Chem.* **1984**, *123*, 335−359.
(41) Kennedy, J. R. M.; Kent, K. E.; Brown, J. R. Rheology of dispersions of xanthan gum, locust bean gum and mixed biopolymer gel with silicon dioxide nanoparticles. *Mater. Sci. Eng., C* **2015**, *48*, 347−353.
(42) Ferry, J. D. *Viscoelastic Properties of Polymers*, 3rd ed.; Wiley: New York, 1980.
(43) Miyazaki, K.; Wyss, H. M.; Weitz, D. A.; Reichman, D. R. Nonlinear viscoelasticity of metastable complex fluids. *Europhys. Lett.* **2006**, *75*, 915−921.
(44) Hyun, K.; Kim, S. H.; Ahn, K. H.; Lee, S. J. Large amplitude oscillatory shear as a way to classify the complex fluids. *J. Non-Newtonian Fluid Mech.* **2002**, *107*, 51−65.

https://doi.org/10.1021/acsomega.1c05382
ACS Omega 2022, 7, 12536−12548

(45) Barnes, H. A. A review of the rheology of filled viscoelastic systems. *Rheol. Rev.* **2003**, *46*, 1−36.
(46) Genovese, D. B. Shear rheology of hard-sphere, dispersed, and aggregated suspensions, and filler-matrix composites. *Adv. Colloid Interface Sci.* **2012**, *171-172*, 1−16.
(47) Gerth, M.; Bohdan, M.; Fokkink, R.; Voets, I.; van der Gucht, J.; Sprakel, J. Supramolecular assembly of self-healing nanocomposite hydrogels. *Macromol. Rapid Commun.* **2014**, *35*, 2065−2070.
(48) Götze, W.; Sjögren, L. β relaxation at the glass transition of hard-spherical colloids. *Phys. Rev. A* **1991**, *43*, 5442.
(49) Meißner, D.; Einfeldt, J. Dielectric relaxation analysis of starch oligomers and polymers with respect to their chain length. *J. Polym. Sci., Part B: Polym. Phys.* **2004**, *42*, 188−197.
(50) Noel, T. R.; Parker, R.; Ring, S. G. Effect of molecular structure and water content on the dielectric relaxation behaviour of amorphous low molecular weight carbohydrates above and below their glass transition. *Carbohydr. Res.* **2000**, *329*, 839−845.
(51) Kaminski, K.; Kaminska, E.; Wlodarczyk, P.; Pawlus, S.; Kimla, D.; Kasprzycka, A.; Paluch, M.; Ziolo, J.; Szeja, W.; Ngai, K. L. Dielectric Studies on Mobility of the Glycosidic Linkage in Seven Disaccharides. *J. Phys. Chem. B* **2008**, *112*, 12816−12823.
(52) Meißner, D.; Einfeldt, J.; Kwasniewski, A. Contributions to the molecular origin of the dielectric relaxation processes in polysaccharides - the low temperature range. *J. Non-Cryst. Solids* **2000**, *275*, 199−209.
(53) Einfeldt, J.; Meißner, D.; Kwasniewski, A. Comparison of the molecular dynamics of celluloses and related polysaccharides in wet and dried states by means of dielectric spectroscopy. *Macromol. Chem. Phys.* **2000**, *201*, 1969−1975.
(54) Hunter, G. L.; Weeks, E. R. The physics of the colloidal glass transition. *Rep. Prog. Phys.* **2012**, *75*, No. 066501.
(55) Ross-Murphy, S. B.; Shatwell, K. P. Polysaccharide strong and weak gels. *Biorheology* **1993**, *30*, 217−227.

https://doi.org/10.1021/acsomega.1c05382
ACS Omega 2022, 7, 12536−12548